

## Research



**Cite this article:** Storelvmo T, Boos WR, Herger N. 2014 Cirrus cloud seeding: a climate engineering mechanism with reduced side effects? *Phil. Trans. R. Soc. A* **372**: 20140116. <http://dx.doi.org/10.1098/rsta.2014.0116>

One contribution of 15 to a Theme Issue 'Climate engineering: exploring nuances and consequences of deliberately altering the Earth's energy budget'.

### Subject Areas:

atmospheric science, climatology, meteorology

### Keywords:

climate engineering, cirrus, ice nucleation, aerosol

### Author for correspondence:

T. Storelvmo

e-mail: [trude.storelvmo@yale.edu](mailto:trude.storelvmo@yale.edu)

# Cirrus cloud seeding: a climate engineering mechanism with reduced side effects?

T. Storelvmo<sup>1</sup>, W. R. Boos<sup>1</sup> and N. Herger<sup>2</sup>

<sup>1</sup>Department of Geology and Geophysics, Yale University, 210 Whitney Avenue, New Haven, CT 06511, USA

<sup>2</sup>Institute for Atmospheric and Climate Science, ETH-Zurich, Zurich, Switzerland

Climate engineering, the intentional alteration of Earth's climate, is a multifaceted and controversial topic. Numerous climate engineering mechanisms (CEMs) have been proposed, and the efficacies and potential undesired consequences of some of them have been studied in the safe environments of numerical models. Here, we present a global modelling study of a so far understudied CEM, namely the seeding of cirrus clouds to reduce their lifetimes in the upper troposphere, and hence their greenhouse effect. Different from most CEMs, the intention of cirrus seeding is not to reduce the amount of solar radiation reaching Earth's surface. This particular CEM rather targets the greenhouse effect, by reducing the trapping of infrared radiation by high clouds. This avoids some of the caveats that have been identified for solar radiation management, for example, the delayed recovery of stratospheric ozone or drastic changes to Earth's hydrological cycle. We find that seeding of mid- and high-latitude cirrus clouds has the potential to cool the planet by about 1.4 K, and that this cooling is accompanied by only a modest reduction in rainfall. Intriguingly, seeding of the 15% of the globe with the highest solar noon zenith angles at any given time yields the same global mean cooling as a seeding strategy that involves 45% of the globe. In either case, the cooling is strongest at high latitudes, and could therefore serve to prevent Arctic sea ice loss. With the caveat that there are still significant uncertainties associated with ice nucleation in cirrus clouds and its representation in climate models, cirrus seeding appears to represent a powerful CEM with reduced side effects.

## 1. Introduction

The practice of cloud seeding goes back to the 1940s, and originally arose as a means to dissipate severe storms or produce precipitation, but numerous dedicated field studies have failed to demonstrate its success [1]. However, cirrus cloud seeding is different from the traditional cloud seeding in many respects: the targeted clouds, the involved microphysical mechanisms and its very intention, which is to modify climate rather than weather. When originally proposed [2], it was assumed that the climate engineering mechanism (CEM) involving cirrus seeding could only be successful if cirrus clouds form via *homogeneous nucleation* in the current atmosphere. Homogeneous nucleation refers to the spontaneous freezing of liquid solution droplets that may occur at sufficiently low temperatures and relative humidity above approximately 150% [3]. By seeding the upper troposphere with efficient ice nuclei (IN) that can form ice crystals at a relative humidity just above saturation, the hypothesis was that homogeneous nucleation could be suppressed. This would prevent freezing of the many solution droplets present in the upper troposphere, and instead ice crystals would form and grow on the few artificial seeds introduced. The purpose of the proposed seeding would be to lower the concentration of ice crystals in cirrus clouds, with the result that they become larger and sediment out more rapidly. The hypothesis that cirrus seeding has the potential to cool climate was supported by a recent atmospheric modelling study, which also reported an optimal seeding amount of approximately  $15\text{ l}^{-1}$  which was sensitive to upper tropospheric dynamics [4].

A setback for this CEM came when *in situ* studies of cirrus clouds over North and Central America reported that they form mainly by *heterogeneous nucleation*, i.e. ice crystals were formed on natural IN consisting predominantly of mineral dust [5]. Although more than half of the cirrus observed derived from convective outflow, the measurements made of cirrus that had formed *in situ* in the upper troposphere still challenged the long-held view that these cirrus clouds form predominantly by homogeneous nucleation. In a recent sensitivity study [6], simulations compatible with the new observations were shown to still yield a significant negative radiative forcing (i.e. a cooling) in response to cirrus seeding. This was possible because homogeneous nucleation still dominated at pristine high latitudes, which also turn out to be the regions where cirrus seeding is most effective. A seeding strategy that required active seeding of only about 45% of the globe was found to yield the same global mean radiative forcing as a globally uniform seeding strategy. By seeding only regions with large solar noon zenith angles, the greenhouse effect of cirrus clouds could be reduced without much compensating warming due to the associated reduction in cirrus cloud albedo.

Here, we present the first coupled atmosphere–ocean model simulations of the climate response to cirrus seeding, and thus go beyond the studies described above, as well as a recent idealized study of the climate response to perturbed ice crystal fall speeds [7]. We present the effect of two different seeding strategies, one that requires seeding of approximately 45% of the globe ('SEEDING') while the other requires seeding of approximately 15% of the globe ('SEEDING2'). These simulations are compared to an unseeded control simulation ('CONTROL'). In all simulations, cirrus clouds may form either by homogeneous or heterogeneous nucleation (or a combination), depending on the conditions of the upper troposphere.

## 2. Methods

The three coupled climate model simulations discussed in this study were run with the Community Earth System Model [8], v. 1.0.4 (CESM1.0.4) of the National Center for Atmospheric Research. CESM1.0.4 is composed of four separate models simulating Earth's atmosphere, ocean, land surface and sea ice. The four components of CESM communicate via a central coupler. The atmospheric model (CAM, v. 5) has been upgraded to allow for supersaturations with respect to ice, and supersaturation frequencies and distributions have been validated [9]. For the purpose of the study of cirrus seeding, the default cirrus parametrization in CAM5 was replaced by an

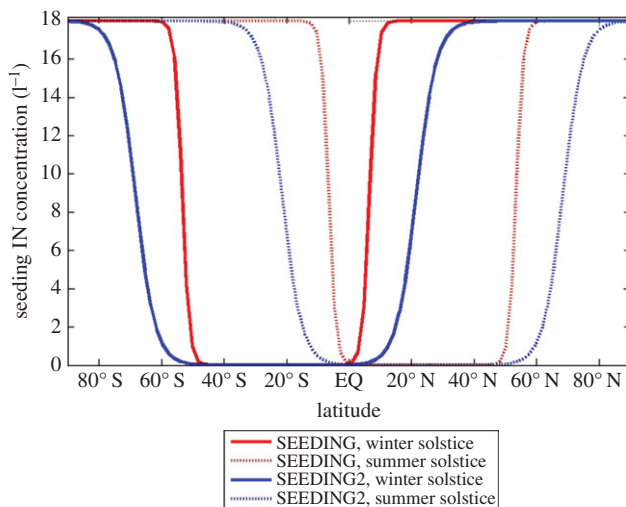


**Figure 1.** The seeding IN concentrations introduced in simulations SEEDING and SEEDING2 as a function of latitude for the summer and winter solstice.

alternative parametrization [10,11]. CAM5 with the alternative parametrization implemented has been validated in terms of upper tropospheric humidity and ice crystal number concentrations in cirrus clouds in a previous study [12]. The simulations were run on a  $f19\_g16$  grid, which corresponds to a finite volume dynamical core, a horizontal atmospheric resolution of  $1.9^\circ \times 2.5^\circ$  and 30 vertical levels, a resolution of approximately  $1^\circ \times 1^\circ$  for the ocean, and a dynamical time step of 30 min. The simulations were integrated for a total of 150 years, starting from a spun-up state corresponding to present-day. Only the last 20 years of the simulations were analysed, and at that point all three simulations had a balanced radiation budget at the top of the atmosphere (TOA) and stable global mean surface air temperatures. The control simulation had a global mean surface air temperature of  $15.4^\circ\text{C}$  and a precipitation rate of  $2.81 \text{ mm d}^{-1}$ , slightly warmer and in reasonable agreement with observations, respectively ( $14.5^\circ\text{C}$  and  $2.68 \text{ mm d}^{-1}$  [13,14]).

In the control simulation, cirrus formation occurred either by homogeneous or heterogeneous nucleation (or a combination), depending predominantly on the temperature, the subgrid-scale vertical velocity (parametrized as a function of turbulent kinetic energy) and the number concentration of mineral dust particles and solution droplets present. We assumed that up to half the mineral dust particles present possessed the ability to act as IN, motivated by laboratory studies showing that not all dust particles have the ability to act as IN [15]. The IN spectrum of the dust particles followed classical nucleation theory with a threshold relative humidity for IN activation of 130% and a contact angle of  $16^\circ$ . The number concentrations of mineral dust, as well as the concentration of solution droplets available for homogeneous nucleation were calculated using the version of the Modal Aerosol Module that describes the aerosol size distribution using three lognormal modes (the Aitken, Accumulation and Coarse modes) [16]. The number of solution droplets available for homogeneous nucleation was set equal to the number of Aitken mode particles, and the dust number concentration of the upper troposphere was taken to be the dust fraction of the Coarse mode.

In the seeded simulations, we prescribed the concentration of seeding IN in the upper troposphere (at temperatures below  $-38^\circ\text{C}$ ) according to the functions displayed in figure 1. We made the seeding IN an increasing function of the solar zenith angle at noon ( $\theta_{S,\text{Noon}}$ ), reflecting scenarios in which the active seeding occurs only over the 15% or 45% largest  $\theta_{S,\text{Noon}}$ , respectively. The imposed decay towards low latitudes reflects our expected efficiency of upper tropospheric meridional mixing of the material in the two cases, and provides an effective forcing over a larger area than that in which active seeding is assumed to occur. Note that while we only display the

seeding functions for summer and winter solstice, there will be a gradual transition between the two throughout the calendar year. The ice nucleation spectrum of the seeding IN was based on classical nucleation theory [11] with a freezing threshold of 105% [2], as has for example been suggested for the artificial IN bismuth tri-iodide ( $\text{BiI}_3$ ). Note that the seeding IN did not affect mixed-phase clouds in the simulations.

No seeding is introduced in regions where the sun is directly overhead at noon, because in these regions the reduction in sunlight reflected due to cirrus thinning exceeds the increased longwave radiation escaping to space, yielding a net warming effect. The fact that the optically thickest tropical cirrus clouds may have a cooling effect as measured at the TOA has previously been reported for radiative transfer calculations [17]. The climate responses to the cirrus seeding were obtained by comparing the equilibrated seeded simulations with the control simulation, designed to be slightly warmer than the present and to have a nearly ice-free summer Arctic. An ice-free summer Arctic has been characterized as an event that would be perceived as alarming enough for CEMs to be seriously considered [18]. A nearly ice-free summer Arctic was recently suggested to occur between 2020 and 2060 [19,20].

### 3. Results

In the control simulations, the relative importance of homogeneous versus heterogeneous ice nucleation (figure 2*a*) is largely controlled by the presence of mineral dust particles. Compared to the control simulations, both seeding simulations suggest that cirrus seeding would have the desired effect of shifting the dominant cirrus formation mode from homogeneous to heterogeneous nucleation, with the most pronounced changes occurring poleward of  $40^\circ$  latitude in both hemispheres (figure 2*b*). As expected, the relatively low dust concentrations in the Southern Hemisphere (SH) cause it to be more susceptible to the seeding. Unfortunately, field observations that can shed light on the relative importance of homogeneous versus heterogeneous ice nucleation poleward of  $50\text{--}60^\circ$  in both hemispheres are virtually non-existent.

In response to the seeding, ice crystal number concentrations in cirrus clouds are drastically decreased in both hemispheres (figure 3*a*), and the increased sedimentation of the fewer but larger ice crystals brings the cloud cover in the upper troposphere down (figure 3*b*). The result is a strong reduction of the cirrus greenhouse effect of as much as  $8\text{--}10\text{ W m}^{-2}$  at high latitudes in both hemispheres. The reduced cirrus cloud albedo compensates for some, but not nearly all, of the increased amount of longwave radiation escaping to space. The net effect leads to a cooling of the entire troposphere (figure 3*c*), and a strong surface cooling that amounts to 1.4 K in the global mean in the SEEDING simulation. Intriguingly, simulation SEEDING2 produces the same global mean cooling, despite a much smaller area of the globe being seeded. We have summarized the global mean changes in key variables relative to CONTROL for both seeding simulations in table 1. As expected, the reduction in the global mean longwave cloud forcing is smaller in SEEDING2 than in SEEDING ( $2.14$  and  $2.80\text{ W m}^{-2}$ , respectively). But by avoiding any shortwave compensation due to the reduction in cloud albedo, SEEDING2 produces a similar change in net cloud forcing to SEEDING. The two simulations have many similar features, so for brevity we will focus only on the differences between the CONTROL and SEEDING simulations in the following. Table 1 also displays hemispheric mean differences between the CONTROL and SEEDING simulations. Evident is a slightly stronger perturbation in the SH than the Northern Hemisphere (NH) for both the cloud and radiation variables.

As the seeding strategy is to target areas with large solar noon zenith angles, the simulated cooling maxima at high latitudes are expected, as is the more modest cooling in the tropics (figure 4*a*). This is in contrast to several studies of solar radiation management (SRM), in which a global mean cooling sufficient to counter the warming due to a doubling of  $\text{CO}_2$  leads to an overcooling of the tropics and an undercooling of the high latitudes [21]. Non-uniform SRM was recently proposed as a remedy for such over- and under-compensation, but how such an optimized distribution of cooling could be achieved was not addressed [22]. Here, the polar amplification factor (PAF), defined as the ratio of polar ( $70\text{--}90^\circ$ ) to global mean surface

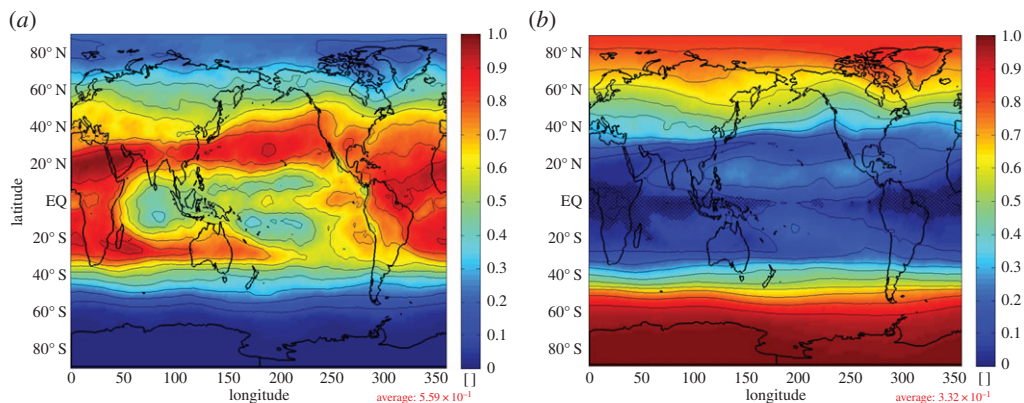


**Figure 2.** (a) The fraction of ice crystals in cirrus clouds at the 200 hPa level that formed by heterogeneous nucleation (HETFRAC) out of the total number of ice crystals formed, from CONTROL and (b) the change in HETFRAC between CONTROL and SEEDING (SEEDING — CONTROL). The hatching indicates regions where the difference between SEEDING and CONTROL is not statistically significant (based on Student's *t*-test with a significance level of 5%).

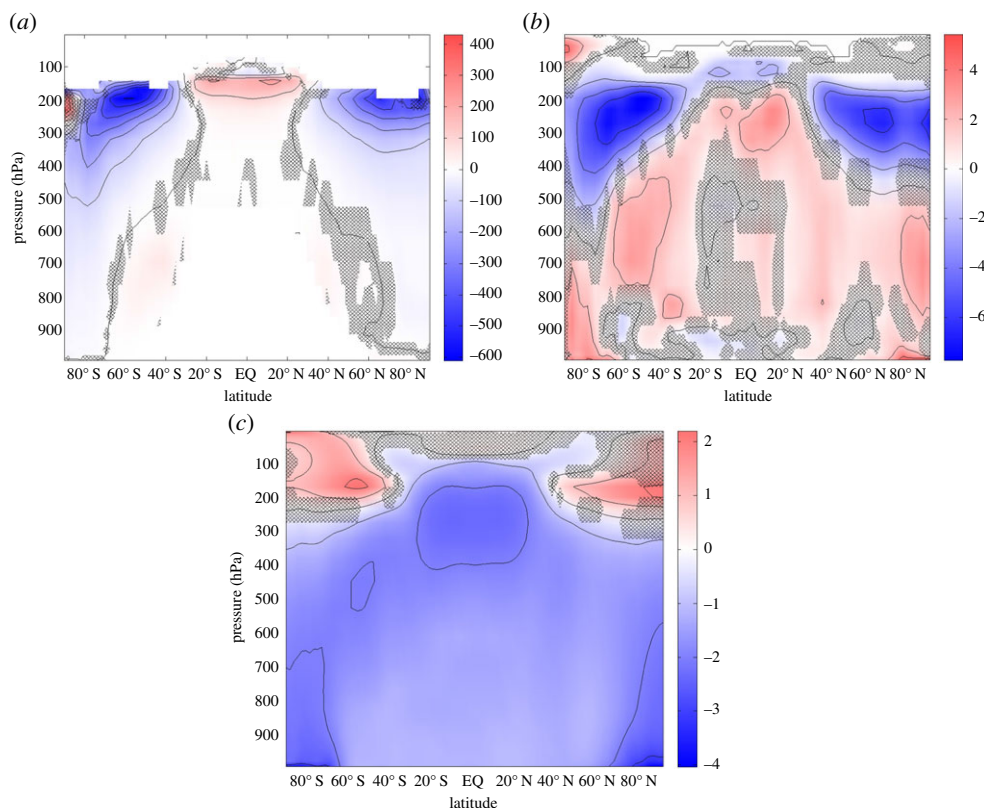


**Figure 3.** (a) The reduction in in-cloud ice crystal number concentration ( $l^{-1}$ ) in response to seeding (SEEDING — CONTROL), and the corresponding changes in (b) cloud cover (%) and (c) temperature (K). The hatching indicates regions where the difference between SEEDING and CONTROL is not statistically significant (applying a Student's *t*-test with a significance level of 5%).

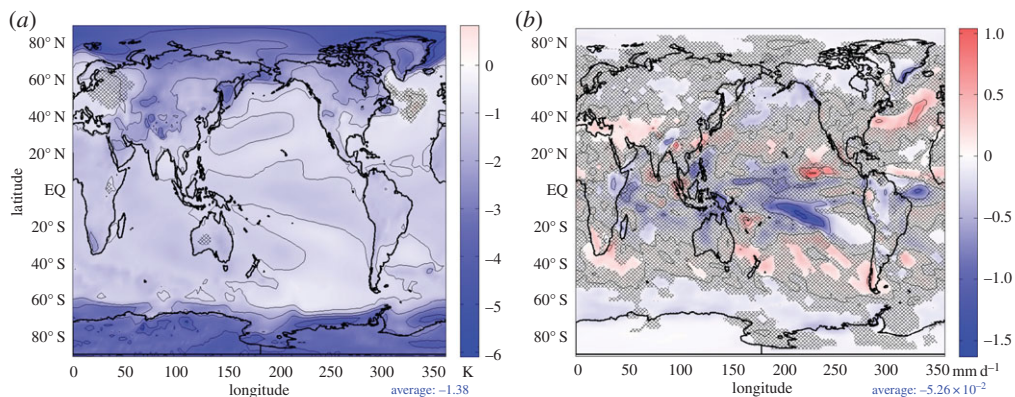


**Figure 4.** (a) The surface air temperature response to seeding (K) and (b) the corresponding change in total (convective and large-scale) precipitation rate (millimetres per day). The hatching indicates regions where the difference between SEEDING and CONTROL is not statistically significant (based on Student's *t*-test with a significance level of 5%).

**Table 1.** Global and hemispheric mean changes in surface air temperature (TS), high cloud cover (CLDHGH), ice water path (IWP), liquid water path (LWP), net cloud forcing (NCF), shortwave cloud forcing (SWCF) and longwave cloud forcing (LWCF) in response to seeding.

$\Delta$	TS (K)	CLD <sub>HGH</sub> (%)	IWP (g m <sup>-2</sup> )	LWP (g m <sup>-2</sup> )	LWCF (W m <sup>-2</sup> )	SWCF (W m <sup>-2</sup> )	NCF (W m <sup>-2</sup> )
SEEDING — CONTROL, global	-1.40	-1.99	-1.59	-0.90	-2.80	0.59	-2.22
SEEDING2 — CONTROL, global	-1.41	-1.71	-1.23	-0.64	-2.14	0.02	-2.11
SEEDING — CONTROL, NH	-1.41	-1.76	-1.28	-0.76	-2.26	0.45	-1.81
SEEDING — CONTROL, SH	-1.39	-2.22	-1.96	-1.09	-3.37	0.78	-2.59

temperature change, is 2.5 and 2.6 for the NH and SH, respectively. This can be compared to PAFs due to a doubling of CO<sub>2</sub> from coupled climate models ranging from 1.5 to 4.5 [23]. The Arctic is central for some of the proposed 'tipping points' in the climate system [24,25], and the cooling efficacy of CEMs at high northern latitudes is therefore of particular interest.

Cooling can be observed for all seasons for the entire globe, with the exception of the North Atlantic. The moderate warming simulated there is the result of an intensification of the Atlantic Meridional Overturning Circulation (AMOC), which strengthens in response to the increased Equator-to-Pole temperature gradient. A similar response of the AMOC has been reported for simulations of the effect of SRM in the form of reflective mirrors installed in space between the Sun and the Earth [26].

Another prominent feature is a stronger cooling of the continents than the oceans for a given latitude band.

The non-uniform seeding strategy, which cools the winter hemisphere more, also influences the onset of the Indian and West African summer monsoons. The increased temperature gradient between the cooler subtropical ocean south of the Equator and the warmer Indian and West African continents triggers earlier monsoon onsets, with anomalously high precipitation rates over the Indian subcontinent and the Sahel region in spring. A similar 'greening' of the Sahel region was found for an asymmetric injection of sulfate aerosols into the SH stratosphere only [27]. By contrast, a modelling study of SO<sub>2</sub> injection into the stratosphere of either the tropics or the Arctic reported a weakening of the monsoons and an associated reduction in rainfall over the Indian subcontinent and the Sahel [28]. A recent multi-model comparison of the hydrological response to SRM also found a significant weakening of monsoon rainfall over Asia and Africa [29].

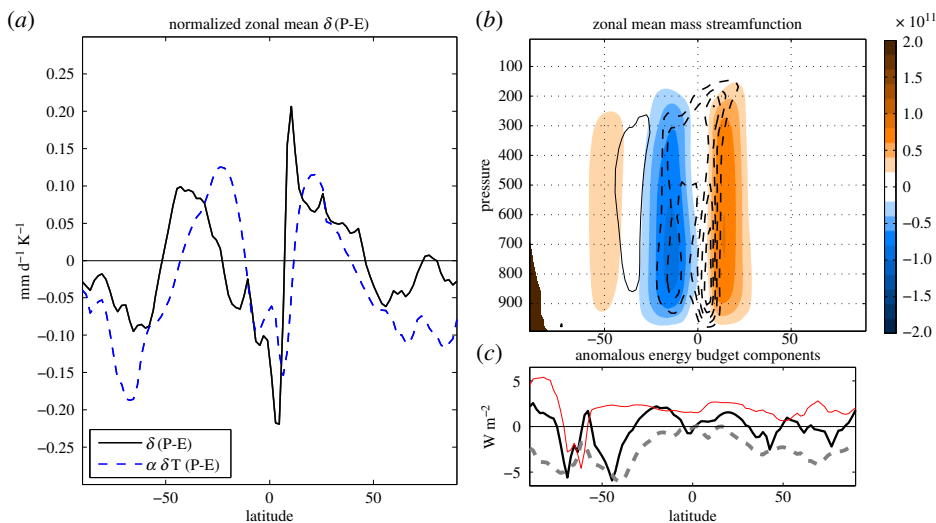


**Figure 5.** (a) Anomalous (SEEDING — CONTROL) zonal mean simulated rate of precipitation minus rate of evaporation (P-E, solid line), and the anomalous P-E predicted by the thermodynamic scaling, both in millimetres per day. (b) Total zonal mean mass streamfunction in the control run (colour shading, contour interval  $10^{10} \text{ kg s}^{-1}$ ) and anomalous zonal mean mass streamfunction (black contours, negative dashed, interval  $2 \times 10^9 \text{ kg s}^{-1}$ , zero contour not shown). Negative contours signify counterclockwise rotation and the black region near the south pole represents topography. (c) Anomalous clear-sky TOA radiative flux (red line, positive downward), anomalous TOA net cloud radiative forcing (dashed line) and anomalous vertically integrated source of atmospheric MSE (thick black line).

Consistent with the effect on the global hydrological cycle reported for other CEMs, we find a reduction in global mean precipitation of  $0.05 \text{ mm d}^{-1}$  in response to the 1.4 K cooling caused by the cirrus seeding. More than 95% of this reduction stems from convective precipitation. However, this reduction is more modest than what is generally reported for SRM. We find a global mean rainfall reduction of  $-1.3\%$  per kelvin of cooling here, versus for example  $-2.4\%$  per kelvin of cooling reported for SRM [30] and a multi-model median of  $1.7\%$  per kelvin of warming reported for a doubling of  $\text{CO}_2$  [31]. The explanation for the different hydrological sensitivity to a cooling arising from shortwave versus longwave radiative forcings is simple [30]: shortwave forcings mainly cool the surface, and thereby reduce surface fluxes of latent heat (i.e. evaporation), which must be balanced by reduced precipitation. Longwave forcings, on the other hand, mainly cool the troposphere (in a direct sense).

Considering only statistically significant precipitation responses, a pattern emerges of ‘dry gets wetter, wet gets drier’: an overall reduction of rainfall over the tropical ocean, a precipitation increase in the subtropics and a decrease at high latitudes (figure 4b). As expected for a global cooling, this precipitation response is opposite of the classical ‘wet gets wetter, dry gets drier’ response to global warming [31,32]. Subtropical semi-arid land regions that experience statistically significant rainfall increase include the Sahel region, the Middle East, the Mediterranean and South Africa. By contrast, some regions with abundant rainfall, like the Amazon and Southeast Asia, get drier. Figure 5 offers further insight into the hydrological response to cirrus seeding; figure 5a shows the simulated zonal mean change in precipitation rate minus evaporation rate (P-E), compared to that predicted by a common thermodynamic scaling [31]. This scaling approximates the vertically integrated atmospheric moisture flux convergence as that which would occur if relative humidity and winds remained fixed as temperatures changed. Under the assumption of fixed lower tropospheric relative humidity, column-integrated water vapour should decrease by about 7% per degree of cooling, as a consequence of the Clausius–Clapeyron relation. The simulated approximately 10% reduction

(not shown) in column-integrated water vapour in response to the 1.4 K cooling is in excellent agreement with that assumption, indicating that any deviation from the thermodynamic scaling will primarily result from changes in winds. Here we calculate the thermodynamic scaling by multiplying the control model's P-E by the product of  $7\% \text{K}^{-1}$  and the zonal mean surface air temperature change at each latitude. This scaling qualitatively matches the simulated change, with reduced P-E in the deep tropics and high latitudes, and increased subtropical P-E (figure 5a).

However, there are some discrepancies between the simulated P-E and that predicted by the thermodynamic scaling. Most notably, there is a northward shift in the intertropical convergence zone (ITCZ), as seen both in the deviation of the simulated P-E from the thermodynamic scaling (figure 5a) and in the anomalous zonal mean mass streamfunction (figure 5b). A meridional ITCZ shift is expected in response to a hemispherically asymmetric energy source [33–35] such as that resulting from cirrus seeding. The hemispheric asymmetry in the anomalous energy source is evident from inspection of the zonal mean radiation budget (figure 5c and table 1). SH cirrus clouds are more susceptible to seeding, because of the virtually dust-free high southern latitudes, so the seeding produces a more negative cloud radiative forcing in the SH. There is also enhanced clear-sky radiative loss in the extratropical SH, between approximately  $70^\circ \text{S}$  and  $60^\circ \text{S}$ , owing to an increase in surface albedo associated with expanded sea ice in the seeded simulation. The enhanced ice albedo response seen in the SH might be a result of the Antarctic being a land mass surrounded by ocean, while the Arctic is an ocean basin surrounded by land [36]. In other words, the expansion of Antarctic sea ice occurs further from the pole and thus may have a stronger annual mean effect on shortwave radiation than the expansion of Arctic sea ice. While the details of ice–albedo interactions merit further investigation, the net effect is that the seeding produces an anomalous energy sink in the extratropical SH, as evidenced by the anomalous vertically integrated source of atmospheric moist static energy (MSE; figure 5c). This anomalous MSE sink must be balanced by a southward transport of MSE from more northern latitudes, which seems to be accomplished by the anomalous Hadley circulation and the ITCZ shift seen in figure 5a,b. While we do not present a full decomposition of the anomalous meridional energy fluxes, this response is generally consistent with previous studies of the tropical response to high-latitude forcings [37].

Finally, there appears to be a slight equatorward shift of the storm tracks (more so in the SH than NH), which acts to increase precipitation in the transition between the subtropics and mid-latitudes. This is analogous to the poleward shift in the storm tracks thought to occur in response to greenhouse warming [38,39]; the cause of such shifts is still the topic of active research.

The long-term hydrologic response to cirrus seeding presented here stands in strong contrast to the dramatic global mean increase in precipitation found when CAM5 is run with fixed climatological sea surface temperatures (SSTs) [6]. The latter can be thought of as the short-term response, after the land and atmosphere have cooled but the SSTs still remain largely unchanged. The increased precipitation rate can be understood as a response to a cooler atmosphere overlaying warm and unchanged SSTs, destabilizing the atmospheric column. Another recent study of aerosol effects on cirrus clouds reported a similar short-term precipitation response, and found it to be closely related to the changes in atmospheric absorption of longwave radiation associated with cirrus clouds [40]. Such opposing short-term and long-term global precipitation responses have previously been reported for other forcing agents, e.g.  $\text{CO}_2$  [41]. An intriguing question, which could be answered with transient climate model simulations, is on what time scales the precipitation change is dominated by the short- versus long-term responses.

Relative to the CEM which has received the most attention so far, namely the SRM scheme involving injection of sulfate aerosols into the stratosphere, cirrus seeding has the advantage that it will not adversely affect stratospheric ozone recovery [42]. While SRM schemes in general act to cool both the stratosphere and the troposphere [43], cirrus seeding would cool the troposphere but warm the stratosphere (figure 3c). The stratospheric warming occurs in response to the increased outgoing longwave radiation leaving the troposphere, of which some is being absorbed in the stratosphere and causes a warming there. Cirrus seeding is hence a less imperfect compensation for increased  $\text{CO}_2$  concentrations than SRM, because it produces a vertical temperature response

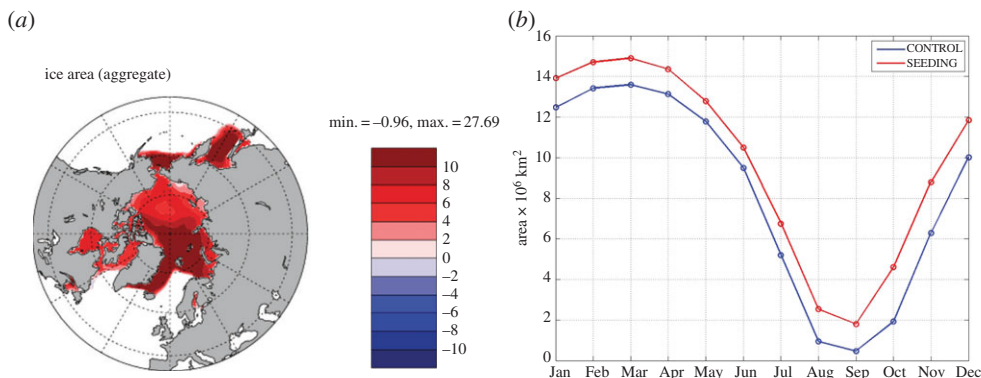


**Figure 6.** (a) Change in annual mean Arctic ice area (%) and (b) the annual cycle of NH sea ice area in simulations CONTROL and SEEDING ( $10^6 \text{ km}^2$ ).

that is similar to that of an increase in  $\text{CO}_2$ , but of opposite sign. Finally, our simulations confirm that Arctic summer sea ice could be recovered by cirrus seeding (figure 6a). The SEEDING simulation produces an Arctic sea ice coverage in the month of September of approximately  $2.0 \times 10^6 \text{ km}^2$ , relative to a nearly ice-free [19] summer Arctic in the CONTROL simulation (figure 6b).

## 4. Discussion

We conclude that while the CEM of cirrus seeding has received little attention so far, the findings presented here warrant further studies. Future research should include laboratory measurements of ice nucleation on the proposed seeding material, and careful evaluations of material toxicity and environmental fate. While determining the optimal delivery method of seeding material to the upper troposphere is beyond the scope of this study, releasing the material using dedicated seeding aircraft appears safer and more viable than adding material to the fuel or exhaust of commercial aircraft, as has previously been suggested [2]. Prior to any implementation, high-resolution simulations of particle dispersion away from the seeding plumes would be required to determine the spacing and frequency of flights required to build up optimal concentrations of seeding material.

Cirrus seeding does not suffer from some of the caveats identified for other CEMs, but it certainly may exhibit its own caveats that have yet to be identified. An easily identifiable caveat is that the current understanding of cirrus clouds, the very targets of the proposed seeding, is still incomplete. This is particularly true for ice nucleation at cirrus levels; the dominant ice nucleation mechanism in high-latitude cirrus is largely unknown, and while one can hypothesize that homogeneous nucleation will dominate at such pristine latitudes and altitudes, that hypothesis has yet to be confirmed. In other words, the results presented here are by no means a sufficient basis for policy decisions at this point. Extensive study of cirrus clouds from space, *in situ* and in numerical models will be required before an implementation of the CEM discussed here could be justified, no matter how unappealing the alternative may appear.

## References

1. Brientjes RT. 1999 A review of cloud seeding experiments to enhance precipitation and some new prospects. *Br. Am. Meteorol. Soc.* **80**, 805–820. (doi:10.1175/1520-0477(1999)080<0805:AROCSE>2.0.CO;2)
2. Mitchell DL, Finnegan W. 2009 Modification of cirrus clouds to reduce global warming. *Environ. Res. Lett.* **4**, 045102. (doi:10.1088/1748-9326/4/4/045102)

3. Koop T, Luo BP, Tsias A, Peter T. 2000 Water activity as the determinant for homogeneous ice nucleation in aqueous solutions. *Nature* **406**, 611–614. (doi:10.1038/35020537)
4. Storelvmo T *et al.* 2013 Cirrus cloud seeding has potential to cool climate. *Geophys. Res. Lett.* **40**, 178–182. (doi:10.1029/2012GL054201)
5. Cziczo DJ *et al.* 2013 Clarifying the dominant sources and mechanisms of cirrus cloud formation. *Science* **340**, 1320–1324. (doi:10.1126/science.1234145)
6. Storelvmo T, Herger N. 2014 Cirrus cloud susceptibility to the injection of ice nuclei in the upper troposphere. *J. Geophys. Res. Atmos.* **119**, 2375–2389. (doi:10.1002/2013JD020816)
7. Muri H, Kristjánsson JE, Storelvmo T, Pfeffer MA. 2014 The climatic effects of modifying cirrus clouds in a climate engineering framework. *J. Geophys. Res. Atmos.* **119**, 4174–4191. (doi:10.1002/2013JD021063)
8. Meehl GA *et al.* 2013 Climate change projections in CESM1(CAM5) compared to CCSM4. *J. Clim.* **26**, 6287–6308. (doi:10.1175/JCLI-D-12-00572.1)
9. Gettelman A *et al.* 2010 Global simulations of ice nucleation and ice supersaturation with an improved cloud scheme in the Community Atmosphere Model. *J. Geophys. Res. Atmos.* **115**, D00M08. (doi:10.1029/2009JD013638)
10. Barahona D, Nenes A. 2008 Parameterization of cirrus cloud formation in large-scale models: homogeneous nucleation. *J. Geophys. Res. Atmos.* **113**, D11211. (doi:10.1029/2007JD009355)
11. Barahona D, Nenes A. 2009 Parameterizing the competition between homogeneous and heterogeneous freezing in cirrus cloud formation—monodisperse ice nuclei. *Atmos. Chem. Phys.* **9**, 369–381. (doi:10.5194/acp-9-369-2009)
12. Liu X *et al.* 2012 Sensitivity studies of dust ice nuclei effect on cirrus clouds with the Community Atmosphere Model CAM5. *Atmos. Chem. Phys.* **12**, 12061–12079. (doi:10.5194/acp-12-12061-2012)
13. Huffman GJ, Adler RF, Bolvin DT, Gu GJ. 2009 Improving the global precipitation record: GPCP Version 2.1. *Geophys. Res. Lett.* **36**, L17808. (doi:10.1029/2009GL040000)
14. Smith TM, Reynolds RW, Peterson TC, Lawrimore J. 2008 Improvements to NOAA's historical merged land–ocean surface temperature analysis (1880–2006). *J. Clim.* **21**, 2283–2296. (doi:10.1175/2007JCLI2100.1)
15. Welti A, Luond F, Stetzer O, Lohmann U. 2009 Influence of particle size on the ice nucleating ability of mineral dusts. *Atmos. Chem. Phys.* **9**, 6705–6715. (doi:10.5194/acp-9-6705-2009)
16. Liu X *et al.* 2012 Toward a minimal representation of aerosols in climate models: description and evaluation in the Community Atmosphere Model CAM5. *Geosci. Model Dev.* **5**, 709–739. (doi:10.5194/gmd-5-709-2012)
17. Fu Q, Baker M, Hartmann DL. 2002 Tropical cirrus and water vapor: an effective Earth infrared iris feedback? *Atmos. Chem. Phys.* **2**, 31–37. (doi:10.5194/acp-2-31-2002)
18. Duarte CM, Lenton TM, Wadhams P, Wassmann P. 2012 Commentary: abrupt climate change in the Arctic. *Nat. Clim. Change* **2**, 60–62. (doi:10.1038/nclimate1386)
19. Overland JE, Wang M. 2013 When will the summer Arctic be nearly ice free. *Geophys. Res. Lett.* **40**, 2097–2101. (doi:10.1002/grl.50316)
20. Liu JP, Song MR, Horton RM, Hu YY. 2013 Reducing spread in climate model projections of a September ice-free Arctic. *Proc. Natl Acad. Sci. USA* **110**, 12571–12576. (doi:10.1073/pnas.1219716110)
21. Kravitz B *et al.* 2013 Climate model response from the Geoengineering Model Intercomparison Project (GeoMIP). *J. Geophys. Res. Atmos.* **118**, 8320–8332. (doi:10.1002/jgrd.50646)
22. MacMartin DG, Keith DW, Kravitz B, Caldeira K. 2013 Management of trade-offs in geoengineering through optimal choice of non-uniform radiative forcing. *Nat. Clim. Change* **3**, 365–368. (doi:10.1038/nclimate1722)
23. Holland MM, Bitz CM. 2003 Polar amplification of climate change in coupled models. *Clim. Dyn.* **21**, 221–232. (doi:10.1007/s00382-003-0332-6)
24. Notz D. 2009 The future of ice sheets and sea ice: between reversible retreat and unstoppable loss. *Proc. Natl Acad. Sci. USA* **106**, 20590–20595. (doi:10.1073/pnas.0902356106)
25. Holland MM, Bitz CM, Tremblay B. 2006 Future abrupt reductions in the summer Arctic sea ice. *Geophys. Res. Lett.* **33**, L23503. (doi:10.1029/2006GL028024)
26. Lunt DJ, Ridgwell A, Valdes PJ, Seale A. 2008 'Sunshade World': a fully coupled GCM evaluation of the climatic impacts of geoengineering. *Geophys. Res. Lett.* **35**, L12710. (doi:10.1029/2008GL033674)
27. Haywood JM, Jones A, Bellouin N, Stephenson D. 2013 Asymmetric forcing from stratospheric aerosols impacts Sahelian rainfall. *Nat. Clim. Change* **3**, 660–664. (doi:10.1038/nclimate1857)

28. Robock A, Oman L, Stenchikov GL. 2008 Regional climate responses to geoengineering with tropical and Arctic SO<sub>2</sub> injections. *J. Geophys. Res. Atmos.* **113**, D16101. (doi:10.1029/2008JD010050)
29. Tilmes S *et al.* 2013 The hydrological impact of geoengineering in the Geoengineering Model Intercomparison Project (GeoMIP). *J. Geophys. Res. Atmos.* **118**, 11 036–11 058. (doi:10.1002/jgrd.50868)
30. Bala G, Duffy PB, Taylor KE. 2008 Impact of geoengineering schemes on the global hydrological cycle. *Proc. Natl Acad. Sci. USA* **105**, 7664–7669. (doi:10.1073/pnas.0711648105)
31. Held IM, Soden BJ. 2006 Robust responses of the hydrological cycle to global warming. *J. Clim.* **19**, 5686–5699. (doi:10.1175/JCLI3990.1)
32. Durack PJ, Wijffels SE, Matear RJ. 2012 Ocean salinities reveal strong global water cycle intensification during 1950 to 2000. *Science* **336**, 455–458. (doi:10.1126/science.1212222)
33. Kang SM, Frierson DMW, Held IM. 2009 The tropical response to extratropical thermal forcing in an idealized GCM: the importance of radiative feedbacks and convective parameterization. *J. Atmos. Sci.* **66**, 2812–2827. (doi:10.1175/2009JAS2924.1)
34. Kang SM, Held IM, Frierson DMW, Zhao M. 2008 The response of the ITCZ to extratropical thermal forcing: idealized slab-ocean experiments with a GCM. *J. Clim.* **21**, 3521–3532. (doi:10.1175/2007JCLI2146.1)
35. Frierson DMW, Hwang YT. 2012 Extratropical influence on ITCZ shifts in slab ocean simulations of global warming. *J. Clim.* **25**, 720–733. (doi:10.1175/JCLI-D-11-00116.1)
36. Eisenman I. 2010 Geographic muting of changes in the Arctic sea ice cover. *Geophys. Res. Lett.* **37**, L16501. (doi:10.1029/2010GL043741)
37. Chiang JCH, Friedman AR. 2012 Extratropical cooling, interhemispheric thermal gradients, and tropical climate change. *Annu. Rev. Earth Planet. Sci.* **40**, 383–412. (doi:10.1146/annurev-earth-042711-105545)
38. Yin JH. 2005 A consistent poleward shift of the storm tracks in simulations of 21st century climate. *Geophys. Res. Lett.* **32**, L18701. (doi:10.1029/2005GL023684)
39. Miller RL, Schmidt GA, Shindell DT. 2006 Forced annular variations in the 20th century Intergovernmental Panel on Climate Change Fourth Assessment Report models. *J. Geophys. Res. Atmos.* **111**, D18101. (doi:10.1029/2005JD006323)
40. Wang M, Liu X, Zhang K, Comstock JM. In press. Aerosol effects on cirrus through ice nucleation in the Community Atmosphere Model CAM5 with a statistical cirrus scheme. *J. Adv. Model. Earth Syst.* (doi:10.1002/2014MS000339)
41. Andrews T, Forster PM, Boucher O, Bellouin N, Jones A. 2010 Precipitation, radiative forcing and global temperature change. *Geophys. Res. Lett.* **37**, L14701. (doi:10.1029/2010GL043991)
42. Mitchell DL, Mishra S, Lawson RP. 2011 Cirrus clouds and climate engineering: new findings on ice nucleation and theoretical basis. In *Planet Earth 2011—global warming challenges and opportunities for policy and practice* (ed. PE Carayannis), pp. 267–288. Rijeka, Croatia: InTech.
43. Caldeira K, Bala G, Cao L. 2013 The science of geoengineering. *Annu. Rev. Earth Planet. Sci.* **41**, 231–256. (doi:10.1146/annurev-earth-042711-105548)